Vanadium redox flow batteries: Potentials and challenges of an emerging storage technology

Vanadium Redox Flow Batteries

Potentials and Challenges of an Emerging Storage Technology

Vanadium redox flow battery (VRFB) systems complemented with dedicated power electronic interfaces are a promising technology for storing energy in smart-grid applications in which the intermittent power produced by renewable sources must face the dynamics of requests and economical parameters. In this article, we review the vanadium-based technology for redox flow batteries (RFBs) and highlight its strengths and weaknesses, outlining the research that aims to make it a commercial success.

Present electric energy production exceeds 10^3 and is growing at a rate of about 3% per year [1]–[3]. For approximately four decades, scientific forecasts warned that conventional resources could not stand this increasing demand in the long term [4], [5], and, only recently, the central administrations of all industrialized countries have embedded into their development programs several policies to gradually replace carbon-based plants with environmentally friendly renewable sources. Following these programs, world wind-generating capacity

reached 369.6 GW in 2014, with an average growth of 18.4% per year in the last five years, and the Global Wind Energy Outlook 2014 forecasts a wind capacity over 750 GW by 2020. The global photovoltaic (PV) capacity grew by 35% in 2013, reaching 177 GW in 2014. The penetration of wind and PV power exceeded 5% in 2014 and is estimated to increase to more than 25% by 2030 [6]–[8]. Unfortunately, renewable sources like wind and solar present two major drawbacks with respect to conventional power plants: they are more expensive and intermittent according to time and climatic conditions. Although the former can be overcome by developing advanced devices based on innovative materials and configurations, the latter calls for suitable energy storage (ES) technologies, grid power is largely oversized or a large energy waste is accepted [9], [10].

The variability of power from renewable sources ranges from the half-day timescale of sunlight typical of PV systems [11] down to the minute-second timescale characterizing wind generators [12], passing through the hourly timescale of tidal power plants [13]. Grid integration of intermittent energy sources requires specific care, as conventional grids can become unstable if power penetration from intermittent sources exceeds 20% of the whole generated power without adequate countermeasures [14]. The most viable solution consists of complementing energy generation from renewables with ES systems, which enable production surplus to be stored during some periods and enhancing delivery when demand is higher [15]–[18].

Additionally, stationary ES systems can provide a number of different services that can be grouped into two main categories depending on their typical timescales: power quality and energy management. The former refers to the charge and discharge cycles on short timescales (seconds to minutes) and includes sag compensation, power smoothing, grid stabilization, and frequency regulation. The latter concerns the charge and discharge cycles on long timescales (hours) and includes load leveling, load following, power balancing, peak shaving, and time shifting, and also contributes toward improving grid-hosting capability [19]. Complementing generation systems with ES presents interesting economic opportunities. When electric utilities offer hourly pricing, ES enables distributors and consumers to reduce their electricity costs. Moreover, large-scale ES, by means of both sparse, large plants and dense, small- to medium-sized systems, can delay upgrades to primary power plants, according to a strategy-of-investment deferral [20]. Depending on these services, operating times range from fractions of a second to several hours, with corresponding response times from milliseconds to several minutes [21], [22], while rated powers vary from a few kilowatts to some gigawatts. Economically convenient and technically competitive storage solutions must have a long calendar life and withstand a large number of charge and discharge cycles.

Storage technologies capable of providing such services are expected to increase dramatically in the near future. A recent authoritative report by the Boston Consulting Group forecasted investments exceeding US$10 billion per year on ES technologies by 2020 [23].

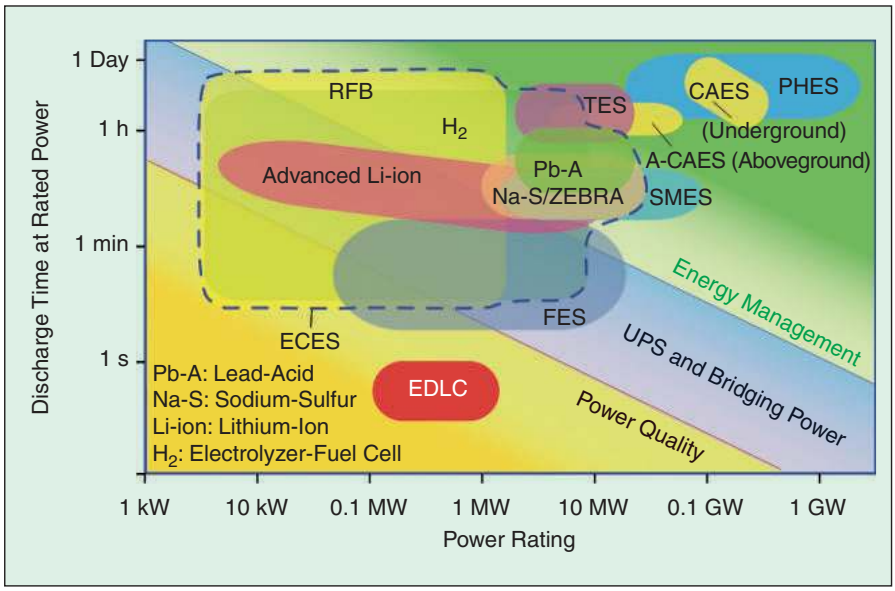

FIGURE 1 – A power-duration diagram of existing ES systems. The blue dotted line encircles ECESs. TES: thermal ES; CAES: compressed air ES; A-CAES: adiabatic compressed air ES; PHES: pumped hydro ES; ZEBRA: Zeolite Battery Research Africa Project (Na-Ni-Cl battery); UPS: uninterruptible power supply.

Presently available ES systems are characterized by different levels of technological development, from emerging to mature, and are suitable for different storage and localization needs. The best performing and most promising storage systems for stationary and mobile electric energy applications are pumped hydro ES, compressed air ES, thermal ES, flywheel ES (FES), superconducting magnetic ES (SMES), and electric double layer capacitor (EDLC) electrochemical ES (ECES). Figure 1

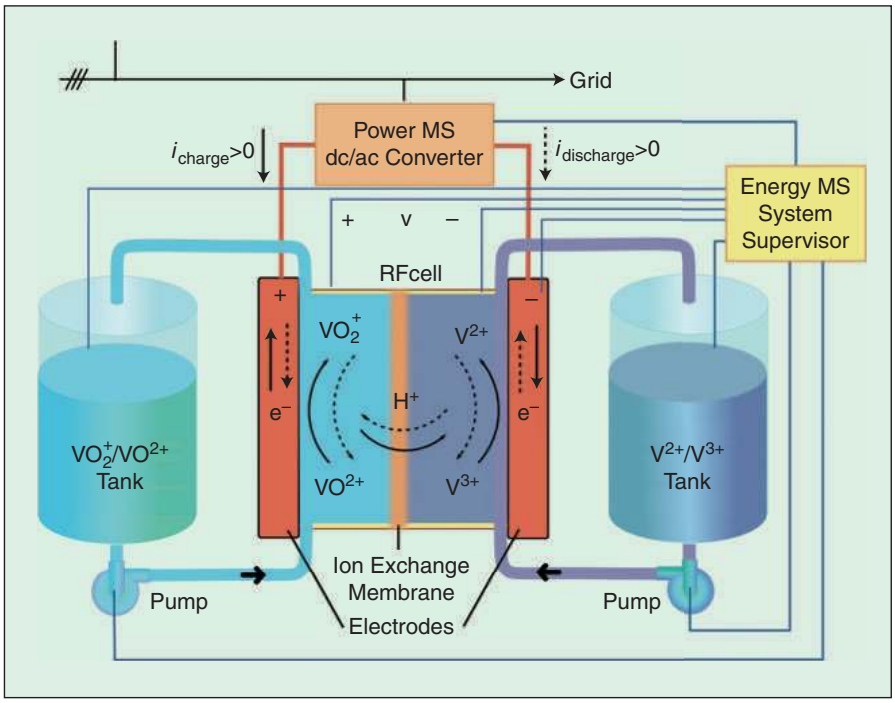

FIGURE 2 – A VRFB scheme. The liquid electrolytes are actively cycled between the cells and tanks by two pumps.

shows how these different technologies are allocated in the power and duration diagram. Currently, the first three kinds are suitable for long-timescale (hours) discharge times, but they cannot cope with fast operations. The first two have tight site constraints, while the third is competitive only when it is used to defer the electric generation of thermo-solar plants. FES, SMES, and EDLC have very fast response times, but are effective on the second-minute timescale and are currently very expensive. SMES are in an early developmental stage; the other two require major improvements to become competitive.

In this framework, several surveys indicate that ECES systems are the solution of choice to provide storage services with wide ranges of discharge times and kilowatt-to-megawatt power ratings because of their large power and energy scalability [23]–[25]. In fact, in the power and duration diagram of Figure 1, they are located in a wide area that is not covered by other storage technologies. These major advantages are complemented by site versatility, very limited environmental impact, modularity, static structure, and ease of operation. Moreover, they are the only ES technologies exploitable on a large scale for electric mobility. Thus, they are expected to spread widely worldwide in the coming years, and substantial funds have been allocated for their future scientific and technological development. Forecasts indicate a growth of the installed power in ES technologies to 330 GW and US$300 billion investments on a global scale by 2030 (250% of today), of which 150 GW (e.g., 45% of the total and 10,000 times the present capacity) will be in ECES technologies with 50% of the total investment [23].

Redox Flow Batteries

Figure 1 shows that a wide area of the power and duration diagram within the ECES is covered by RFBs. The principle behind them is a couple of electrochemical reduction and oxidation reactions occurring in two liquid electrolytes that contain metal ions. Both half-cells where the reactions occur are connected to external storage tanks where the solutions are circulated by means of pumps (Figure 2). This feature provides RFBs with an almost unique advantage over other ECES systems: power and energy ratings are independent. Table 1 compares the main figures of the more competitive electrochemical ES technologies presently available, including VRFBs, which are currently the marketed version of RFBs. Cost figures are obtained from contracts recently signed for a multitechnology ES facility under construction in Venice, Italy, and show that present commercial VRFBs are already very competitive compared with other ECES technologies.

In this framework, RFBs are emerging as a promising option for stationary ES in electric grids with regard to both power quality and energy management services [9]. In addition

TABLE 1 – THE MAIN DATA OF COMPETING ELECTROCHEMICAL STORAGE TECHNOLOGIES FOR STATIONARY SERVICES.

ECES TECHNOLOGY	ENERGY DENSITY [WH/KG]	DISCHARGE TIME [H]	RESPONSE TIME	ROUND-TRIP EFFICIENCY	CYCLE LIFE ·10³	CAPEX [K€/KW]	CAPEX [€/KWh]	CAPEX [C€/KWH/CYCLES]
Advanced Pb-acid	25–50	1–2	ms	75%	0.8	1.9	770	96.3
Na-S	150–120	2–6	ms	89%	4.5	3.6	450	10.0
Na-Ni-Cl	95–120	0.5–2	ms	90%	4.5	3.55	1638	36.4
Li-ion	100–200	1	ms	87%	4.0	0.71	1246	31.1
H_2 electrolyzer/FCs	800–1300	>10	10^2 ms	24%	0.3	7.1	<1880	<626.7
VRFB	24	>10	ms	75%	20	2.65	<663	<4.4

Costs include ancillaries (discharge times are at rated power; cost figures based on 2015 commercial contracts; capex = capital expenditure).

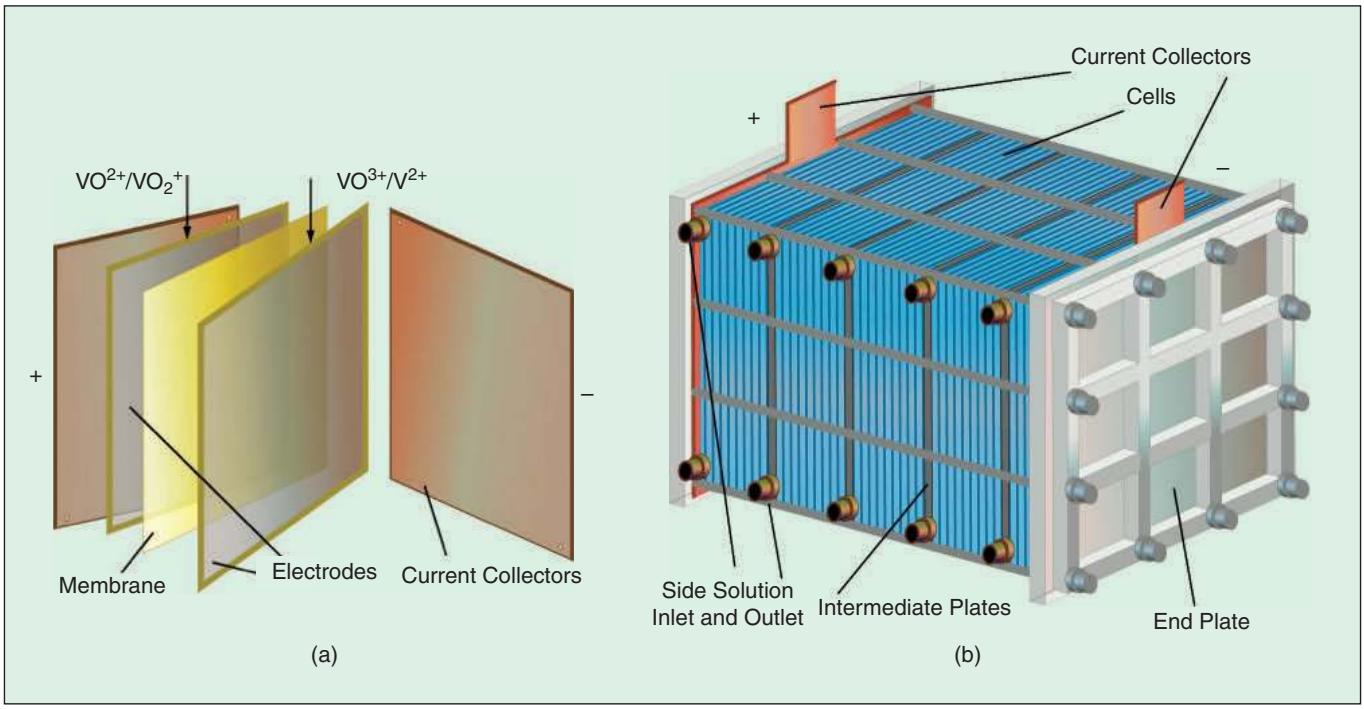

FIGURE 3 – (a) The internal view of an RFB cell showing a central polymer electrolyte membrane, two porous electrodes, and two graphite current collectors. (b) A sketch of a typical VRFB stack, made of *N* cells connected in direct series through bipolar plates.

to sharing the aforementioned advantages with the other ECESs (lead-acid, lithium, sodium-sulfur, sodium-nickel-chlorine, nickel-metal, etc.), their power- and energy-independent sizing allows for long discharge times unachievable with other ECESs (unless those ECESs are largely oversized in power). RBFs have response times in the order of milliseconds, high overloading for short times, good round-trip efficiency, room-temperature operation, low self-discharge, and an extremely long charge and discharge lifecycle. They are fully reversible since the same device performs both charge and discharge. For several features, they are similar to fuel cells (FCs), which are also power and energy independent, but are not reversible (they need an electrolyzer for converting electricity into hydrogen where the energy is stored), exhibit much lower round-trip efficiency, have a shorter lifecycle, and are more expensive.

RFBs store energy in two electrolytic solutions containing different redox couples, depending on the used chemistry. In some cases, one solution is substituted with gas or air. The battery heart is a stack made of several cells, each formed of two electrodes separated by an ion-conducting electrolyte [Figure 3(a)]. The electrodes consist of compartments, into which the electrolytic solutions are pumped and the half-electrochemical reactions take place during operation. The electrolyte is a polymeric membrane that prevents electrolytic solutions from mixing and allows the passage of ions but not electrons. The solutions are circulated through their external tanks by means of two pumps. Similarly to FCs, this architecture decouples power rating, which depends on the stack size, from stored-energy rating, which depends on the tank's volume. The overall stack structure is shown in Figure 3(b).

Several chemistries can be used in RFBs (many of which are under investigation), including both aqueous and nonaqueous solutions, such as vanadium-vanadium, bromine-polysulphide, zinc-bromine, zinc-cerium, magnesium-vanadium, vanadium-cerium, vanadium-polyhalide, vanadium-bromine, vanadium-oxygen, and hydrogen-bromine. Other chemistries, such as quinone-bromide (based on organic quinones) are also being investigated, but they appear much more exotic and far from competitive industrial exploitation. Although some promising results have been obtained with other chemistries, the all-vanadium chemistry (V-V) used in the VRFBs is the best developed option so far. It was introduced in the 1970s and, though having already been commercialized, several aspects of its operation remain to be explored and improved [26]. A VRFB exploits the four oxidation states of vanadium, with V(II) (bivalent V^{2+}) and V(III) (trivalent V^{3+}) used at the negative electrode, and V(IV) (tetravalent VO^{2+}) and V(V) (pentavalent VO_2^+) at the positive electrode (the bright colors of the four oxidation states are shown in Figure 4). These ions are dissolved with concentrations of 1.5–2 M in an aqueous solution of sulfuric acid, with concentration of 2–5 M. The electrochemical half-reactions are:

$$VO^{2+} + H_2O \underset{\text{discharge}}{\overset{\text{charge}}{\rightleftharpoons}} VO_2^+ + 2H^+ + e^-$$

negative electrode

$$V^{3+} + e^- \underset{\text{discharge}}{\overset{\text{charge}}{\rightleftharpoons}} V^{2+}. \qquad (1)$$

The ions $2H^+$ (protons) move through the membrane to maintain the electrical neutrality of the electrolytes and, in doing so, they close the electric current circulation, whereas the electrons produce it in the external circuits.

Economically convenient and technically competitive storage solutions must have a long calendar life and withstand a large number of charge and discharge cycles.

The cell eletrodes where the half-reactions of (1) occur are typically made of highly porous carbon or graphite felts, treated to improve their hydrophilicity and to achieve catalytic effects. Complex mass transport effects occur inside the electrodes, involving diffusion, convection, and migration, according to the Nernst-Plank equation. The ions migrating through the polymer membrane electrolyte are protons H^+ if a cationic membrane is used, or anions (e.g., bisulfate HSO_4^-) if an anionic membrane is adopted.

Cell Voltage

Half-reactions (1) produce a cell-reversible voltage, namely, an electromotive force (emf), of $E^0 = 1.26$ V at $T_o = 298.15$ K (25 °C), and with balanced molar concentrations c_x of the two reacting species x in each electrode. In real operating conditions, the emf E deviates from E^0 because of the operating temperature T and the variations of the concentrations c_x, according to the Nernst equation. In turn, the concentrations c_x of the two species in each electrode vary linearly with the state of charge (SOC) in a complementary way so as to maintain their sum constant, neglecting side effects. Moreover, E is also affected by the proton concentration on each face of the membrane, which depend on the SOC [27]. The cell emf depends on the SOC s ($s = 0$ at full discharge and $s = 1$ at full charge) as

$$E(s) = E^{0'} + \frac{2RT}{F} \ln \frac{s}{1-s}, \qquad (2)$$

where $E^{0'} = 1.37$ V is a corrected standard emf that accounts for proton concentrations and corresponds to $s = 0.5$, R is the universal gas constant, T is the absolute temperature, and F is the Faraday's constant. Figure 5(a) shows how E varies with s according to (2). Neglecting side effects (e.g., species crossover, discussed later) and with a good approximation, E coincides with the cell's open circuit voltage (OCV) so that, based on (2), a simple measure of the OCV can provide the SOC of the solutions [28]. This technique is simple to implement, even if it lacks precision for intermediate SOC values, due to the local low value of the curve slope and to side effects, such as ion crossover. Moreover, it is more precise at higher and lower SOC, where the slope increases and where the control of SOC is more crucial to avoid dangerous over- and undercharges.

In both charge and discharge load conditions, the cell voltage v_c differs from the OCV (2) due to voltage drops Δv_i (> 0 in discharge mode, or voltage decrease, and < 0 in charge mode, or voltage increase) which depend on the current density j in the cell active area. Such voltage drops depend on several effects, such as electrochemical activation related to the reaction kinetics, species concentration gradients in the electrodes, and ohmic losses due to the membrane ionic resistivity [Figure 5(b)].

Cell and Stack Sizing

The required cell current i_c is achieved by properly sizing the cell cross-sectional area $A = i_c/j_r$. Because the rated current density j_r can reach 0.1–0.15 A/cm^2 in modern commercial devices, cell areas can exceed 50 cm × 50 cm to generate currents in the order of 10^2 A. In comparison, FCs, which exploit similar cell architecture, have areas at least tenfold smaller, thanks to current densities in excess of 1 A/cm^2. Similarly to all other ECESs, the voltage v_c of a VRFB cell [Figure 5(b)] is too low for practical uses, calling for the series connection of N cells so as to achieve a stack voltage $v_s = N v_c$. Properly sizing A and N allows the rated current and voltage—and thus, the rated power—to be achieved. The typical solution to create the series, inspired by FC technology, consists of piling N cells into a stack by interposing a bipolar plate between two next cells, as shown in Figure 3(b). This bipolar plate, usually made of graphite, creates the electrical connection between two cells while separating the positive solution of one cell from the negative solution of the adjacent cell. Holes in the bipolar plates form manifolds inside the stack that provide parallel distribution and collection of the solutions inside all cell electrodes.

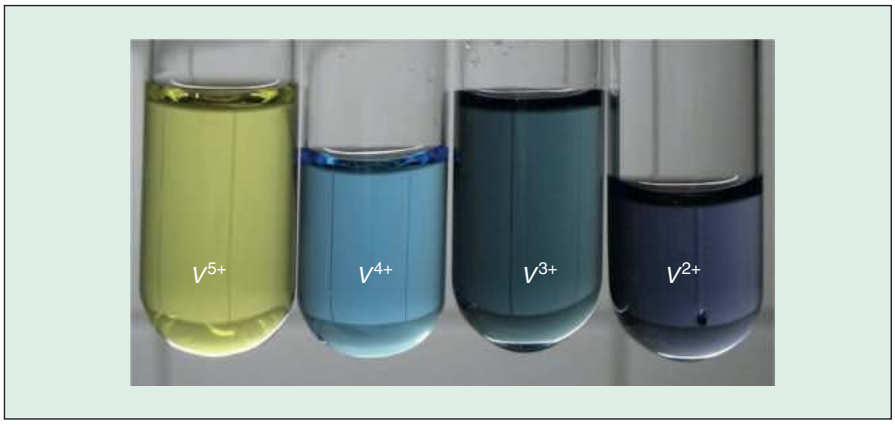

FIGURE 4 – Vanadium exhibits the notable feature of presenting four oxidation states, characterized by different brilliant colors. (Image courtesy of homescience.net; http://woelen.homescience.net/science/index.html.)

Side Effects and Challenges

Crossover Effects

Although VRBs are already commercialized in large systems, up to the

4 MW/6 MWh plant built by Sumitomo Electric Industries (Japan) for J-Power in 2005, research is underway to overcome their present limits to fully exploit them commercially [29]. Crossover involves unwanted diffusive and electro-osmotic transfer of vanadium ions, bisulfate, and water through the membrane. The former effect depends on the concentration gradients between the two electrodes, whereas the latter is driven by the ion motion through the membrane. Consequently, in addition to crossover varying with the different species according to their diffusivity and mobility, the two effects also occur with different intensities depending on the SOC, and the latter reverses direction in charge and discharge [30], [31]. The overall effect is that charge and discharge cycle after cycle crossover produces a net transfer of vanadium from one compartment to the other, causing a solution imbalance and reducing the battery capacity [32]. Moreover, water crossover from one compartment to the other can cause vanadium salt precipitation if solubility limits are exceeded. For these reasons, crossover calls for control and corrective measures, the easiest being a periodical redistribution of the solutions between the positive and negative compartments, the more challenging being the smart design of the cell membranes.

Forecasts indicate a growth of the installed power in ES technologies to 330 GW and US$300 billion investments on a global scale by 2030.

Pumping Losses and Shunt Currents

Two more major issues arise with VRFBs because they work on liquid electrolytic solutions, unlike FCs working on gaseous hydrogen and oxygen. First, the higher viscosity and larger cell cross-sections of liquid reactants imply higher pressure drops and pumping powers, which impact battery efficiency. Second, electric currents flow inside the conducting solutions along the homologous electrodes that are at different electrical potentials and fed hydraulically in parallel. These so-called shunt currents depend on the temperature, as usual in electrolytic conductors, and also on the concentrations of the species that have different conductivity and vary with the SOC. The joule losses due to shunt currents occur in both stand-by and load conditions, reducing the stored energy. Apart from thermodynamic constraints and internal cell voltage drops, pumping losses and shunt currents are primarily responsible for stack losses and round-trip efficiency limitation. Because reducing the pumping power calls for short and large piping, whereas reducing the shunt currents calls for long and thin piping, these two issues pose conflicting constrains that can be addressed with advanced stack channel and manifold designs identified by means of computational fluid dynamics combined with numerical optimizers [33].

Power and Energy Densities

Another major issue of VRFBs is their low power and energy densities: 0.15 W/cm^2 in the cells, 100 W/kg in the stack, and 25 Wh/kg in the solutions, which imply large stacks and tanks. These sizes can be acceptable in stationary applications, but they are a drawback with respect to other devices (e.g., lithium-ion batteries exceed

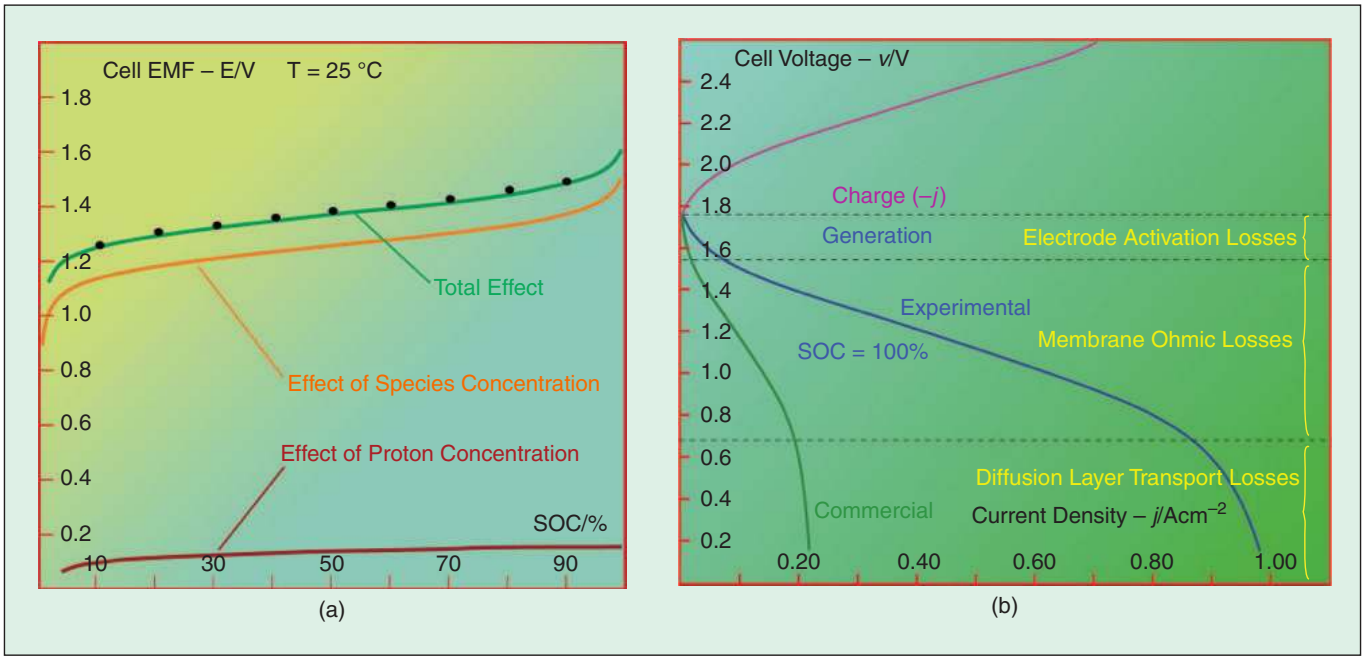

FIGURE 5 – VRFB-cell voltage: (a) emf, which is basically the OCV, as a function of the SOC with experimental data from [28]. (b) The polarization curve (load voltage as a function of the cell current density at SOC = 100%).

Pumping losses and shunt currents are primarily responsible for stack losses and round-trip efficiency limitation.

300 W/kg and 200 Wh/kg). More compact systems exhibiting higher power and energy densities will resort to nonaqueous electrolytic solutions or improved electrode activity, but vanadium aqueous solutions can also undergo important progresses [34]. In fact, cell power densities exceeding 0.55 W/cm^2 have already been reported in small size tests [35], and energy densities fourfold higher than present seem at hand. The achievement of these targets stems from new materials for both the porous electrodes and the polymeric membrane. Higher power and energy densities will involve not only smaller devices, but also lower costs and lower inhomogeneity of the physical quantities across the cell area and among the cell forming the stack, which will increase the overall performance.

Present-day commercial VRFBs, with their modest 25–50 Wh/kg, are not suitable for mobility use, but the previously mentioned improvements are also promising in this regard. More compact future RFB systems could be competitive for powering electric vehicles, allowing for driving ranges greater than those seen today with battery electric vehicles and with refueling as fast and easy as gasoline.

Cell and Stack Modeling

The careful evaluation of cell and stack performance must account for electrochemical, fluid-dynamic, electrical, and thermal effects. Nonlinear equations are used to achieve this, notably the Butler-Volmer equation to model the electrochemical kinetics and activation overpotentials (i.e., voltage drops in electrical terms) as a function of the current density, the Nernst-Plank equation for mass and ion transport in the electrodes, and the Vogel-Tamman-Fulcher equation for ion transport in the membrane.

Advanced models of mass transport in the electrode, such as the Lattice-Boltzmann, can capture the nonlinear superdiffusive meso-scale ion behavior in the anisotropic porous media [36]. Based on this set of equations, several multiphysics models have been developed to compute RFB (and, notably, VRFB) electric performance as a function of the varying species concentrations, mass flow rate, and temperature, taking into account electrodes' and membranes' physical-chemical properties. Increasingly accurate models have been developed that also account for the side effects, such as species crossover through the membrane and solution imbalance. When the large cells of industrial systems have to be studied, two- and three-dimensional models must be used to account for the gradients of the physical quantities across the cell area. This is challenging because of the prevalently two-dimensional geometries (consisting of strata of thin layers) with aspect ratios exceeding 1,000, which imply an extremely critical domain tessellation when approached with conventional finite element techniques and call for a high-level simulation package, notably Comsol and Fluent, and in-house software, such as proper generalized decomposition [37]. However, such models are quite complex, and their description goes beyond the scope of this article. More information can be found in the recent literature [38], [39].

On the other hand, a detailed spatial analysis is not needed when modeling the VRFB interfaces with the power converter to connect to the grid and with the system supervisor [also referred to as energy management system (MS)] that is devoted to real-time monitoring and control of the power converter and active components (e.g., pumps and valves) to ensure the best efficiency in every operating condition. Much simpler models are used in this case, such as reduced-complexity equivalent circuits, which capture the major effects occurring in a VRFB.

One example is shown in Figure 6(a), where the controlled voltage source represented the fem E expressed in (2) [40]. The resistances represent the losses due to conduction in the membrane (m), electrochemical activation in the positive and negative electrodes ($a+$, $a-$), and mass flow in the electrodes (d). The capacitors account for the double-layer effects at the reaction surfaces inside the electrodes. The four controlled current sources represent the species crossover from one electrode to the other, which are driven by diffusion ($cd+$, $cd-$) and electro-osmotic drag ($ce+$, $ce-$). The controlled current source (pump) accounts for the power absorption from the circulating pumps and the equivalent resistor (shunt) for the shunt currents in the solutions. Equivalent circuits like these also allow extended and unscented Kalman filters to be derived to estimate the VRFB SOC [41].

At the simplest level, it can be noted that electrochemical activation losses are much lower than the membrane ohmic losses at full load, while concentration losses are important when the rated current density j_r is exceeded. Thus, to determine the electrical requirements for the power MS (namely, the interface power electronics) design, the major effect to consider is the resistive voltage drop in the membrane, which can be expressed in per-unit area quantities as

$$\Delta v_m = r_m j = (d/\sigma) j, \qquad (3)$$

where r_m is the specific membrane resistance; d is its thickness, kept at a minimum; and σ its conductivity. As usual in electrolytic conductors, σ strongly increases with temperature. A typical value at normal operating temperature (20–30 °C) is $r_m = 1.5\ \Omega\text{cm}^2$. This value can be increased by 80%–100% to account for other loss effects, leading to a prudential equivalent total specific resistance $r_t = 3\ \Omega\text{cm}^2$, which

allows a simple estimation of the cell voltage as

$$v_c \cong E(s) - \Delta v_t = E(s) - r_t j. \quad (4)$$

The corresponding simplified equivalent circuit is shown in Figure 6(b).

Future RFB systems could be competitive for powering electric vehicles, allowing for driving ranges greater than those seen today with battery electric vehicles and with refueling as fast and easy as gasoline.

Vanadium Redox Flow Battery MS, Supervisor, and Power Electronics

The current literature lacks specific studies dedicated to optimal VRFB system management, including its ancillaries (e.g., pumps, valves), and to power electronics solutions that can cope with the unique features of these kinds of electrochemical systems. A system supervisor, or MS, is needed that could coordinate control of the electrical, chemical, and fluid-dynamic quantities according to the electric input and output power requirements. Even if they do provide effective operations, actual supervisors of commercial VRFBs are not always fully optimized from the point of view, for instance, of the overall losses and of the round-trip efficiency. The VRFB MS would need SOC and state of health (SOH) online data to ensure optimized overall system control that allows it to meet power exchange expectations with the grid and load, to increase reliability, and to extend the stack's lifetime [42] to improve its dynamic performances at the same time.

SOC online monitoring allows electrolyte rebalancing when needed. In VRFBs, cross-contamination between the two half-cells is not critical because both the positive and the negative sides contain vanadium, but, unfortunately, the crossover phenomena described in the "Crossover Effects" section does occur. The resulting concentration imbalance appears especially after long-term cycling and permanently reduces overall capacity, which is counteracted by electrolyte rebalancing. The literature reports VRFB SOC monitoring methods based on coulomb counting, by requiring expensive instrumentation or some computationally heavy models, which are not easy or cheap to implement in commercial VRFB systems. Some other approaches to VRFB SOC evaluation are based on OCV measurements [43] or on Kalman filters [44]. Evaluating VRFB SOH estimation is problematic. It is afforded, although without well-assessed results, in the case of lithium batteries [45] and FCs [46] through electrochemical impedance spectroscopy, which is now the subject of on-field applications through cheap and reliable electronics [47].

The mean for SOC/SOH online data is, as often happens for FCs [47], the switching converter, whose main function is to interface the VRFB to the external world. Its main features, which make it unique for VRFB applications, are its wide input voltage range, its ability to cover charging and discharging operations, and its bidirectionality. As in the case of lithium batteries and FCs, the topological solution, consisting in

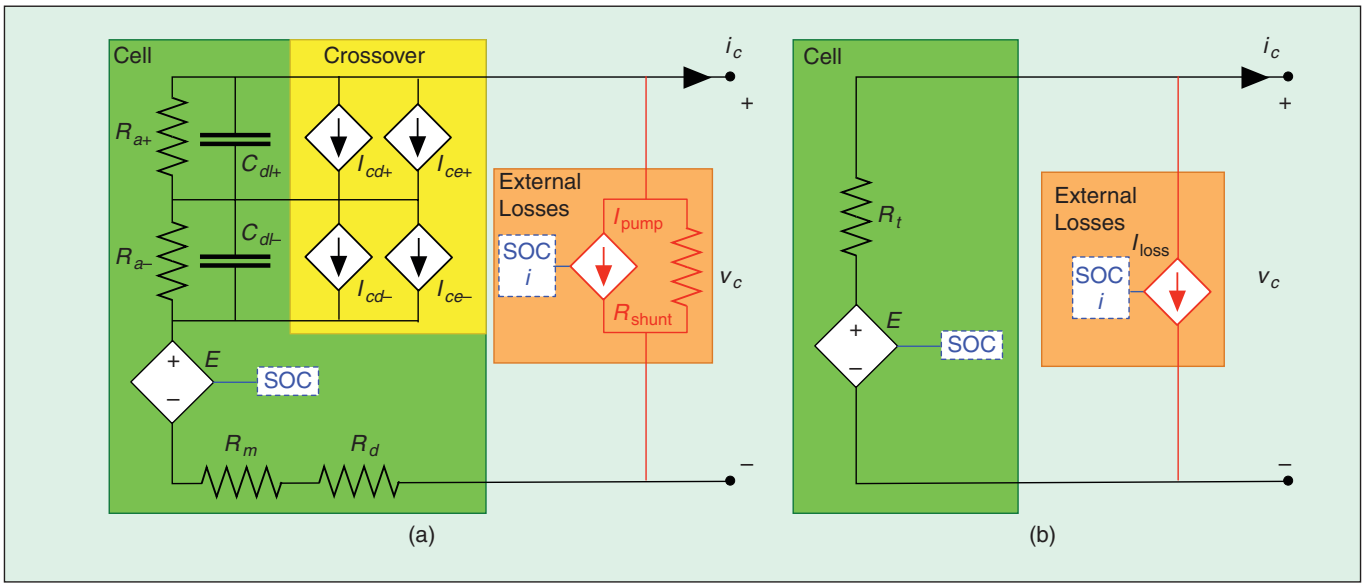

FIGURE 6 – The equivalent circuits of a VRFB cell. (a) In detail, E is the SOC emf. R_{a+}, R_{a-}, R_m, and R_d represent the internal losses due to electrochemical activation in the positive and negative electrodes, conduction in the membrane, and mass flow in the electrodes, respectively. C_{dl+} and C_{dl-} account for the double layer electrostatic effects at the reaction surfaces. I_{cd+}, I_{cd-}, I_{ce+}, and I_{ce-} represent species crossover driven by diffusion and electro-osmotic drag, respectively. I_{pump} accounts for the pumping power needed for circulating the solutions, that depends on both cell current I and SOC, and R_{shunt} accounts for the shunt currents. (b) Simplified, R_t is a Thévenin equivalent resistor accounting for all cell internal losses, whereas I_{loss} accounts for all external losses (shunt currents and pumping).

TABLE 2 – MAIN FEATURES OF THE MOST PROMISING POWER CONVERTER ARCHITECTURES.

REF	ARCHITECTURE	TOPOLOGY	HF TRANSFORMER	SOFT-SWITCHING	PROS	CONS	CONTROL METHOD
[49]–[51]	DAB	Half or full bridge	Single or three phase	ZVS	High-power density/reduced-output filter	High circulating currents for backflow power, hard switching at light loads, tight input voltage range, discontinuous input current	Phase-shift modulation/dual- and triple-phase-shift modulation/ frequency modulation
[49]–[51]	DAB with resonant tank	Half or full bridge	Single or three phase	LC cell, T-type LCL, CLLC cells	Backflow power minimization, switching-losses reduction	High circulating currents for backflow power, hard switching at light loads, tight input voltage range, discontinuous input current	Phase-shift modulation/dual- and triple-phase-shift modulation/ frequency modulation
[49]	Isolated bidirectional converters	Dual-flyback, dual-Cuk, zeta-sepic, forward-flyback	Center tap	Snubber circuits	Reduced number of switches	The power density depends on the number of switches	Phase-shift + PWM control
[52]	Current-fed DAB	Full bridge	Three phase	ZVS/naturally clamped	High efficiency over a wide input voltage range, low transformer turn ratio	Turn-off voltage spike, snubber circuits or active clamp circuitry are recommended	Phase-shift/duty-cycle control, current-mode control
[55] and [56]	Current-fed DAB	Resonant push-pull/ interleaved boost	Center tap/coupled inductors	ZCS-ZVS	High reliability, low cost compared to the active-clamped ZVS solutions	Turn-off voltage spike, snubber circuits or active clamp circuitry are recommended	Unique duty-cycle modulation for forward/reverse power flow control

ZVS: zero voltage switching; ZCS: zero current switching; PWM: pulse width modulation; LC: inductive-capacitive.

a cascade of two stages (a dc/dc and a dc/ac), allows flexibility to realize an interface with renewable energy sources, such as a PV, having a high voltage bus. The dc/ac converter allows for smart grid connection. Dc/ac topologies for grid connection of renewable sources is a common topic in the literature (e.g., [48]), but these articles often refer to unidirectional and not isolated solutions. The more challenging issues are dc/dc topology and control. The main features of the most promising solutions have been summarized in Table 2.

The phase-shift dual active bridge (DAB) is a very good candidate for implementing the dc/dc power stage employed in VRFB MS [49] (Figure 7). Adopting a high-frequency transformer embedded into the dc/dc converter topology allows galvanic isolation and a high-voltage conversion ratio at the same time. The phase-shift modulation allows a change to the current in the filter inductance (L) by acting on the displacement between the square-wave voltages appearing at the output of the left-side bridge and at the input of the right-side bridge. The sign and magnitude of the phase-shift angle determine the direction and the amount of the transferred power, respectively. In fact, by referring to the ac side of the active bridges and by assuming that they are operating as a sinusoidal system for the sake of simplicity, it is

$$P = \frac{V_1 V_2 \sin\delta}{X}, \qquad (5)$$

where V_1 and V_2 are the amplitude of the first harmonic of the line-to-line voltages at the two sides of the inductance, its reactance thereof being X, and δ is the angle of displacement between the two sinusoidal waves.

The DAB can also include clamping circuits and resonant tanks to achieve soft-switching operation mode, high-conversion efficiency, and reduced component stresses (the basic scheme is shown in Figure 8). Some examples of tank circuits are reviewed in [49], starting from the classic inductive-capacitive

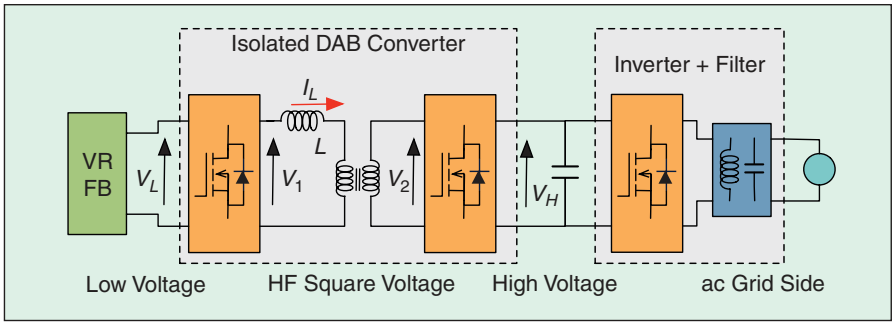

FIGURE 7 – A phase shift DAB [49].

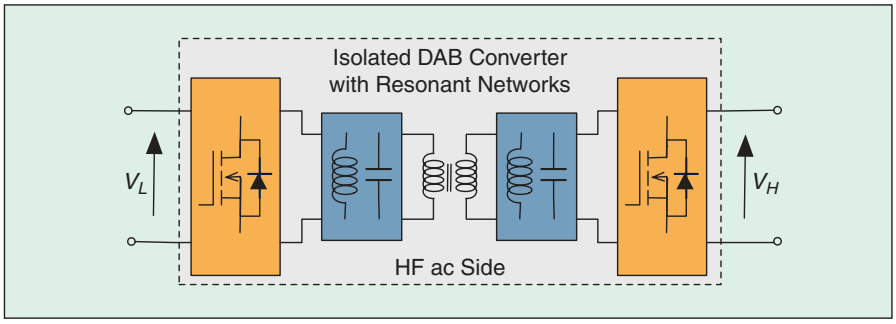

FIGURE 8 – A phase shift DAB with resonant tanks.

(LC) type, showing that the parasitic parameters can save additional components. As noted therein, once the switch voltage and current ratings are fixed, the DAB's power transmission capability is proportional to the number of switches. For instance, two half-bridge topologies, which involve a total of four switches, have twice the power transmission capability of configurations based on single-switch converters (e.g., dual-flyback or dual-Cuk converters), but halved with respect to the dc/dc converters, which use two full bridges and require eight switches. For this reason, and because of the ripple at the double of the switching frequency it produces, a DAB with two full bridges is preferred, especially for high-power applications. The DAB efficiency also depends on how the two bridges are controlled; this is studied in-depth in [50], which considers a 2-kW automotive application.

Especially in high-power applications, as in centralized VRFB storage system solutions for smart grids, the relatively low VRFB output voltage requires that the upstream bridge input is split so multiphase and interleaved configurations can manage currents as high as some hundreds of amperes. These solutions also offer the advantage of a reduced VRFB current ripple, so bulky and heavy filtering elements are avoided and the electrolytic capacitors' lifetime is increased. Three-phase DAB topology reduces the component stress, but requires a three-phase symmetrical transformer having almost identical leakage inductances in each phase [51], [52].

A current-fed resonant push-pull DAB (PP-DAB), which adopts a novel modulation strategy allowing operation in bidirectional mode, has recently been presented [53]. It meets the needs of a VRFB, but its conversion efficiency depends too much on voltage input variations.

Some interesting features are shown by the solution recently presented in [54], which has some similarities with the PP-DAB, especially because of the wide range of input voltage, low current ripple, and soft switching capabilities. The interleaved boost with coupled inductors converter is an isolated topology suitable for high step-up applications. A unidirectional solution is presented and analyzed in [54], both in steady state and by deriving a small signal model that might be used for control purposes. This solution needs to be extended to a bidirectional case and validated at more than a few hundred watts.

Even if they do provide effective operations, actual supervisors of commercial VRFBs are not always fully optimized.

Similarly to lithium batteries and FCs, VRFBs suffer from mismatching problems related to uneven aging and behavior of the cells connected to each other to form the large stack. Although high-power VRFBs are actually commercialized for centralized storage solutions, some efforts are made to design modular solutions that reduce the mismatching impact and allow the plant to scale up easily. One example is the product commercialized by Proxhima [55] and shown in Figure 9. VRFB modularity means independent vanadium vessels, but also a low-power, bidirectional, dc/dc converter dedicated to each battery element. From an architectural point of view, the dc/dc converter output terminals can be connected in series or in parallel to form the desired array, with distributed control solutions that have been extensively studied in the field of PV systems [56]. As for dc/dc converter topologies, in this low-power (e.g., kilowatt) application, the current-fed DAB is the most promising because it ensures, with respect to the voltage-fed DAB, lower root mean square current and zero voltage switching in the whole operating range, thus reaching high efficiency values. Current-fed solutions are preferred as active bridges on the VRFB side, where the input voltage is greatly sensitive to the charge and discharge operating mode. The experimental results given in [52], which refer to a three-phase topology, show a conversion efficiency in the range of 92–96%, with the VRFB operating voltage ranging in 24–48 V, the output voltage fixed at 288V, and a transferred power in the range 1–5 kW.

Conclusions

Stationary ES will be a key feature of future smart grids and micro grids because it can provide them with a number of service capabilities, ranging from power quality to energy management. In this framework, RFBs are emerging as a very competitive option due to their unique advantages. Moreover, RFBs present interesting margins of improvement, and the developments pursued in many laboratories can boost their adoption in the near future.

Two major side effects hampering the efficiency of these devices are

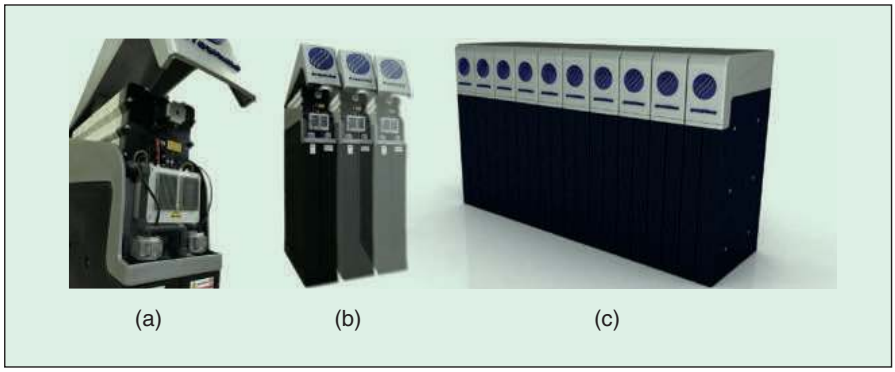

FIGURE 9 – The Proxhima VR 24-C6 modular VRFB. Each unit is rated 4 kW, 64–40 V, 24 kWh. (a) The unit internal arrangement with the 4-kW stack placed over the tanks, (b) the system modular concept, and (c) the arrangement of a 40-kW, 240-kWh system. (Photo courtesy of Proxhima.)

A DAB with two full bridges is preferred, especially for high-power applications.

shunt currents in the electrolyte solutions and pumping power. New stack topologies are being investigated that will reduce these effects, with the goal of increasing efficiency by 10% (so as to exceed 80%) and approaching the figures now provided by lithium- and sodium-based batteries. A promising solution relies on the stack topology suggested some years ago, but never investigated nor tested, according to the existing literature, that involves connecting the cells in parallel within a stack [57]. This method may minimize shunt currents inside the stack while keeping the pressure drop and the pumping power low. A major contributor to RFBs' success can come from the industrial electronics area, which can develop advanced, high-efficiency power MSs capable of low-voltage, high-current, bidirectional operations while coping with VRFB voltage variation (Figure 5). Integrated multivariable control systems capable of ensuring highly efficient and versatile operations are also key to the market success of the next RFBs.

Biographies

Massimo Guarnieri earned his M.S. degree (honors) in electrical engineering from the University of Padua, Padova, Italy, in 1979 and his Ph.D. degree in electrical science in Rome in 1987. He joined the Italian National Council of Research in 1982 and the University of Padua in 1983, where he has been full professor of electrical engineering since 2000. Initially, he worked on devices for thermonuclear fusion research. He later centered his interests on electromagnetic numerical computation. In the last ten years, he has been involved in modeling and designing electrochemical storage devices. He is interested in the history of technology and science. His scientific production of more than 200 items (more than 100 indexed by Scopus) includes several textbooks. He holds three patents. He represents the University of Padua in N.ERGHY, the European Union Research Association in the Fuel Cell and Hydrogen Joint Technology Initiative. He is a columnist and a member of the editorial board of *IEEE Industrial Electronics Magazine*.

Paolo Mattavelli earned his Ph.D. degree in electrical engineering from the University of Padua, Padova, Italy, in 1995. Since 1995, he has had faculty positions at the Universities of Padua, Udine, and Virginia Polytechnic Institute and State University in Blacksburg. He is currently a professor with the University of Padua, leading the power electronics laboratory in Vicenza. His major field of interest includes analysis, modeling and control of power converters, grid-connected converters for renewable energy systems and smart-grids, and high-temperature and high-power density power electronics. In these research fields, he has been leading several industrial and government projects. He is a Fellow of the IEEE.

Giovanni Petrone earned his M.S. degree in electronic engineering from the University of Salerno, Italy, in 2001 and his Ph.D. degree in electrical engineering from the University of Napoli "Federico II," Italy, in 2004. Since 2014, he has been an associate professor in the Department of Electrical Engineering at the University of Salerno, where he teaches circuit theory and power electronic circuits for renewable energy sources. His main research interests are in the analysis and design of switching converters for telecommunication applications and renewable energy sources, modeling and control of photovoltaic, fuel cell and battery systems, and maximum power point tracking algorithms. He is a coauthor of more than 100 papers published in international journals and conference proceedings, four patents, and a book devoted to renewable sources applications. He is a Member of the IEEE.

Giovanni Spagnuolo (gspagnuolo@unisa.it) earned his M.S. degree in electronic engineering from the University of Salerno, Italy, in 1993 and his Ph.D. degree in electrical engineering from the University of Napoli "Federico II," Italy, in 1997. Since 2016, he has been a full professor of electrical engineering at the University of Salerno. He is in the Thomson Reuters 2015 list of the Most Influential Researchers and is an editor of *IEEE Journal of Photovoltaics* and an associate editor of *IEEE Transactions on Industrial Electronics*. His main research interests are in photovoltaics and in renewable energy systems, in general, in storage systems and in power electronics. He is a Fellow of the IEEE.

References

[1] International Energy Agency. (2013, Nov. 12). World energy outlook 2013. Paris, France. [Online]. Available: http://www.worldenergyoutlook.org/weo2013/

[2] International Energy Agency. (2012). 2012 key world energy statistics. Paris, France. [Online]. Available: http://www.iea.org/publications/freepublications/

[3] U.S. Energy Information Administration. (2013, Apr.). Annual energy outlook 2013: With projections to 2040. U.S. Department of Energy. Washington, D.C. [Online]. Available: www.eia.gov/forecasts/aeo/pdf/0383(2013).pdf

[4] D. H. Meadows, D. L. Meadows, J. Randers, and W. W. Behrens, III, "The limits to growth," in *Green Planet Blues: Critical Perspectives on Global Environmental Politics*, 5th ed., K. Conca and G. D. Dabelko, Eds. Boulder, CO: Westview Press, 1972.

[5] K. S. Deffeyes, *Hubbert's Peak: The Impending World Oil Shortage*. Princeton, NJ: Princeton University Press, 2008.

[6] European Commission, "Proposal for a council decision establishing the specific programme implementing Horizon 2020—the framework programme for research and innovation (2014–2020)," Brussels, Belgium, COM(2011) 811 final, 2011/0402 (CNS), 2013.

[7] S. Chu and A. Majumdar, "Opportunities and challenges for a sustainable energy future," *Nature*, vol. 488, no. 7411, pp. 294–303, Aug. 2012.

[8] J. M. Barrosos. (2014, July 9). JTI launch event 2014–2020 speech. [Video file]. Retrieved from https://www.youtube.com/watch?v=Acn4Pry7g6A

[9] P. Alotto, M. Guarnieri, and F. Moro, "Redox flow batteries for the storage of renewable energy: A review," *Renew. Sust. Energ. Rev.*, vol. 29, pp. 325–335, Jan. 2014.

[10] S. Vazquez, S. M. Lukic, E. Galvan, L. G. Franquelo, and J. M. Carrasco, "Energy storage systems for transport and grid applications," *IEEE Trans. Ind. Electron.*, vol. 57, no. 12, pp. 38,881–33,895, Dec. 2010.

[11] P. Poggi, G. Notton, M. Muselli, and A. Louche, "Stochastic study of hourly total solar radiation in Corsica using a Markov model," *Int. J. Climatol.*, vol. 20, no. 14, pp. 1843–1860, Nov. 2000.

[12] A. Sturt and G. Strbac, "Efficient stochastic scheduling for simulation of wind-integrated

power systems," *IEEE Trans. Power Syst.*, vol. 27, no. 1, pp. 323–334, Feb. 2012.

[13] C. M. Johnstone, D. Pratt, J. A. Clarke, and A. D. Grant, "A techno-economic analysis of tidal energy technology," *Renew. Energy*, vol. 49, pp. 101–106, Jan. 2013.

[14] E. J. Coster, J. M. A. Myrzik, B. Kruimer, and W. L. Kling, "Integration issues of distributed generation in distribution grids," *Proc. IEEE*, vol. 99, no. 1, pp. 28–39, Jan. 2011.

[15] J. M. Carrasco, L. C. Franquelo, J. T. Bialasiewicz, E. Galván, R. C. Portillo Guisado, M. A. Martín Prats, J. I. León, and N. Moreno-Alfonso, "Power-electronic systems for the grid integration of renewable energy sources: A survey," *IEEE Trans. Ind. Electron.*, vol. 53, no. 4, pp. 1002–1016, Aug. 2006.

[16] J. Kondoh, I. Ishii, H. Yamaguchi, A. Murata, K. Otani, K. Sakuta, N. Higuchi, S. Sekine, and M. Kamimoto, "Electrical energy storage systems for energy networks," *Energy Conv. Manag.*, vol. 41, no. n. 17, pp. 1863–1874, Nov. 2000.

[17] B. P. Roberts and C. Sandberg, "The role of energy storage in development of smart grids," *Proc. IEEE*, vol. 99, no. 6, pp. 1139–1144, June 2011.

[18] T. Hennessy, "Overcoming transmission constraints: energy storage and Wyoming wind power. DOE energy storage systems research program annual peer review," Washington, D.C., Nov. 2006.

[19] J. P. Barton and D. G. Infield, "Energy storage and its use with intermittent renewable energy," *IEEE Trans. Energy Convers.*, vol. 19, no. 2, pp. 441–448, June 2004.

[20] R. Poudineh and T. Jamasb, "Distributed generation, storage, demand response and energy efficiency as alternatives to grid capacity enhancement," *Energy Policy*, vol. 67, pp. 222–231, Apr. 2014.

[21] S. Sundararagavan and E. Baker, "Evaluating energy storage technologies for wind power integration," *Sol. Energy*, vol. 86, pp. 2707–2717, Sept. 2012.

[22] A. Zahedi, "Maximizing solar PV energy penetration using energy storage technology," *Renew. Sust. Energ. Rev.*, vol. 15, pp. 866–870, Jan. 2011.

[23] C. Pieper and H. Rubel, "Revisiting energy storage. There is a business case," Boston Consulting Group Report, Feb. 2011.

[24] W. F. Pickard, A. Q. Shen, and N. J. Hansing, "Parking the power: Strategies and physical limitations for bulk energy storage in supply–demand matching on a grid whose input power is provided by intermittent sources," *Renew. Sust. Energ. Rev.*, vol. 13, pp. 1934–1945, Oct. 2009.

[25] B. Dunn, H. Kamath and J. Tarascon, "Electrical energy storage for the grid: a battery of choices," *Science*, vol. 334, no. 6058, pp. 928–935, Nov. 2011.

[26] G. L. Soloveichik, "Flow batteries: Current status and trends," *Chem. Rev.*, vol. 115, no. 20, pp. 11,533–11,558, Sept. 2015.

[27] K. Knehr and E. Kumbur, "Open circuit voltage of vanadium redox flow batteries: Discrepancy between models and experiments," *Electrochem. Commun.*, vol. 13, no. 4, pp. 342–345, Apr. 2011.

[28] B. Xiong, J. Zhao, Z. Wei, and M. Skyllas-Kazacos, "Extended Kalman filter method for state of charge estimation of vanadium redox flow battery using thermal-dependent electrical model," *J. Power Sources*, vol. 262, pp. 50–61, Sept. 2014.

[29] A. Parasuraman, T. M. Lim, C. Menictas, and M. Skyllas-Kazacos, "Review of material research and development for vanadium redox flow battery applications," *Electrochim. Acta*, vol. 101, pp. 27–40, July 2013.

[30] S. Won, K. Oh, and H. Ju, "Numerical analysis of vanadium crossover effects in all-vanadium redox flow batteries," *Electrochim. Acta*, vol. 177, pp. 310–320, Sept. 2015.

[31] X. G. Yang, O. Ye, P. Cheng, and T. S. Zhao, "Effects of the electric field on ion crossover in vanadium redox flow batteries," *Appl. Energy*, vol. 145, pp. 306–319, May 2015.

[32] K. Ngamsai and A. Arpornwichanop, "Analysis and measurement of the electrolyte imbalance in a vanadium redox flow battery," *J. Power Sources*, vol. 282, pp. 534–543, May 2015.

[33] S. König, M. R. Suriyah, and T. Leibfried, "Model based examination on influence of stack series connection and pipe diameters on efficiency of vanadium redox flow batteries under consideration of shunt currents," *J. Power Sources*, vol. 281, pp. 272–284, May 2015.

[34] S. Kim, E. Thomsen, G. Xia, Z. Nie, J. Bao, K. Recknagle, W. Wang, V. Viswanathan, O. Luo, X. Wei, A. Crawford, G. Coffey, G. Maupin, and V. Sprenkle, "1 kW/1 kWh advanced vanadium redox flow battery utilizing mixed acid Electrolytes," *J. Power Sources*, vol. 237, pp. 300–309, Sept. 2013.

[35] D. S. Aaron, Q. Liu, Z. Tang, G. M. Grim, A. B. Papandrew, A. Turhan, T. A. Zawodzinski, and M. M. Mench, "Dramatic performance gains in vanadium redox flow batteries through modified cell architecture," *J. Power Sources*, vol. 206, pp. 450–453, May 2012.

[36] D. Maggiolo, F. Picano, A. Marion, and M. Guarneri, "Application of the Lattice-Boltzmann method for modeling all-vanadium redox flow batteries," in *Proc. IV Int. Conf. Particle-Based Methods—Fundamentals and Applications—Particle 2015,* Sept. 28–30, 2015, pp. 579–589.

[37] P. Alotto, M. Guarnieri, F. Moro, and A. Stella, "Multi-physic 3D dynamic modelling of polymer membranes with a proper generalized decomposition model reduction approach" *Electrochim. Acta*, vol. 57, no. 1, pp. 250–256, Dec. 2011.

[38] Q. Xu and T. S. Zhao, "Fundamental models for flow batteries," *Progr. Energy Combust. Sci*, vol. 49, pp. 40–58, Aug. 2015.

[39] Q. Zheng, X. Li, Y. Cheng, G. Ning, F. Xing, and F. Zhang, "Development and perspective in vanadium flow battery modeling," *Appl. Energy*, vol. 132, pp. 254–266, Nov. 2014.

[40] X. Qiu, T. A. Nguyen, J. D. Guggenberger, M. L. Crow, and A. C. Elmore, "A field validated model of a vanadium redox flow battery for microgrids," *IEEE Trans. Smart Grid*, vol. 5, no. 4, pp. 1592–1601, July 2014.

[41] B. Xiong, J. Zhao, Z. Wei, and M. Skyllas-Kazacos, "Extended Kalman filter method for state of charge estimation of vanadium redox flow battery using thermal-dependent electrical model," *J. Power Sources*, vol. 262, pp. 50–61, Sept. 2014.

[42] M. J. Watt-Smith, P. Ridley, R. G. A. Wills, A. A. Shah, and F. C. Walsh, "The importance of key operational variables and electrolyte monitoring to the performance of an all vanadium redox flow battery," *J. Chem. Technol. Biotechnol*, vol. 88, no. 1, pp. 126–138, Jan. 2013.

[43] K. Ngamsai and A. Arpornwichanop, "Analysis and measurement of the electrolyte imbalance in a vanadium redox flow battery," *J. of Power Sources*, vol. 282, pp. 534–543, May 2015.

[44] V. Yu, A. Headley, and D. Chen, "A constrained extended Kalman filter for state-of-charge estimation of a vanadium redox flow battery with crossover effects," *ASME. J. Dyn. Sys., Meas., Control*, vol. 136, no. 4.

[45] P. Gao, C. Zhang, and G. Wen, "Equivalent circuit model analysis on electrochemical impedance spectroscopy of lithium metal batteries," *J. Power Sources*, vol. 294, pp. 67–74, Oct. 2015.

[46] C. de Beer, P. S. Barendse, and P. Pillay, "Fuel cell condition monitoring using optimized broadband impedance spectroscopy," *IEEE Trans. Ind. Electron*, vol. 62, no. 8, pp. 5306–5316, Aug. 2015.

[47] Project HEALTH-CODE. Real operation pem fuel cells HEALTH-state monitoring and diagnosis based on dc-dc Converter embedded EIS. H2020-JTI-FCH-2014-1. [Online]. Available: http://www.pemfc.health-code.eu

[48] S. Kouro, J. I. Leon, D. Vinnikov, and L. G. Franquelo, "2Grid-connected photovoltaic systems: An overview of recent research and emerging PV converter technology," *IEEE Ind. Electron. Mag.*, vol. 9, no. 1, pp. 47–61, March 2015.

[49] B. Zhao, O. Song, W. Liu, and Y. Sun, "Overview of dual-active-bridge isolated bidirectional dc–dc converter for high-frequency-link power-conversion system," *IEEE Trans. Power Electron.*, vol. 29, no. 8, pp. 4091–4106, Aug. 2014.

[50] F. Krismer and J. W. Kolar, "Efficiency-optimized high-current dual active bridge converter for automotive applications," *IEEE Trans. Ind. Electron.*, vol. 59, no. 7, pp. 2745–2760, July 2012.

[51] R. W. A. A. De Doncker, D. M. Divan, and M. H. Kheraluwala, "A three-phase soft-switched high-power-density DC/DC converter for high-power applications," *IEEE Trans. Ind. App.*, vol. 27, no. 1, pp. 63–73, Jan./Feb. 1991.

[52] Z. Wang and H. Li, "A soft switching three-phase current-fed bidirectional dc-dc converter with high efficiency over a wide input voltage range," *IEEE Trans. Power Electron.*, vol. 27, no. 2, pp. 669–684, Feb. 2012.

[53] J. Hiltunen, V. Vaisanen, and P. Silventoinen, "A bidirectional current-fed resonant push-pull converter for low voltage, high current applications," in *Proc. 2013 IEEE Energy Conversion Congr. Exposition*, Sept. 15–19, 2013, pp. 4770–4774.

[54] G. Spiazzi and S. Buso, "Analysis of the interleaved isolated boost converter with coupled inductors," *IEEE Trans. Ind. Electron.*, vol. 62, no. 7, pp. 4481–4491, July 2015.

[55] Proxhima. [Online]. Available: http://www.proxhima.com

[56] N. Femia, G. Petrone, G. Spagnuolo, and M. Vitelli, *Power Electronics and Control Techniques for Maximum Energy Harvesting in Photovoltaic Systems*, Boca Raton, FL; CRC Press, 2013.

[57] P. M. Spaziante, "Novel design and non-conventional applications for vanadium redox technology," presented at the International Redox Flow Battery Forum, Vienna, Austria, June 15–16, 2010.